

Magnetic memory and distinct spin populations in ferromagnetic $\text{Co}_3\text{Sn}_2\text{S}_2$

Charles Menil,¹ Brigitte Leridon,¹ Antonella Cavanna,² Ulf Gennser,² Dominique Mailly,²
Linchao Ding,³ Xiaokang Li,³ Zengwei Zhu,³ Benoît Fauqué,⁴ and Kamran Behnia¹

¹*Laboratoire de Physique et d'Étude des Matériaux
(ESPCI - CNRS - Sorbonne Université)
Université Paris Sciences et Lettres, 75005 Paris, France*

²*Centre de Nanosciences et de Nanotechnologies, CNRS,
Université Paris-Saclay, 91120 Palaiseau, France*

³*Wuhan National High Magnetic Field Center and School of Physics
Huazhong University of Science and Technology, Wuhan 430074, China*

⁴*JEIP (USR 3573 CNRS), Collège de France
Université Paris Sciences et Lettres, 75005 Paris, France*

(Dated: September 19, 2024)

$\text{Co}_3\text{Sn}_2\text{S}_2$, a ferromagnetic Weyl semi-metal with Co atoms on a kagome lattice, has generated much recent attention. Experiments have identified a temperature scale below the Curie temperature. Here, we find that this magnet keeps a memory, when not exposed to a magnetic field sufficiently large to erase it. We identify the driver of this memory effect as a small secondary population of spins, whose coercive field is significantly larger than that of the majority spins. The shape of the magnetization hysteresis curve has a threshold magnetic field set by the demagnetizing factor. These two field scales set the hitherto unidentified temperature scale, which is not a thermodynamic phase transition, but a crossing point between meta-stable boundaries. Global magnetization is well-defined, even when it is non-uniform, but drastic variations in local magnetization point to a coarse energy landscape, with the thermodynamic limit not achieved at micrometer length scales.

I. Introduction

First synthesized as a ternary chalcogenide with Shandite structure [1], $\text{Co}_3\text{Sn}_2\text{S}_2$ became a subject of tremendous attention after its identification as a ferromagnetic Weyl semi-metal [2, 3]. It crystallizes in a rhombohedral structure with $R\bar{3}m$ space group ($n^\circ 166$). The cobalt atoms form kagome sheets in the ab plane, which are separated by blocks of Sn and S atoms (see Figure 1a). It magnetically orders below $T_C \approx 175$ K with a saturation moment of $\approx 0.3 \mu_B$ per Co atom [4], and with the easy axis residing along the c -axis. *Ab initio* band calculations [5], as well as photoemission [6] and Mössbauer experiments [7] identified it as a ferromagnetic half-metal. It is also a semi-metal with an equally low concentration of electrons and holes ($n = p \simeq 8.7 \times 10^{-19} \text{cm}^{-3}$ [8]). Thanks to such a low carrier density (comparable to elemental antimony, where $n = p \simeq 6.6 \times 10^{-19} \text{cm}^{-3}$), mobility is sufficiently large to detect quantum oscillations and experimentally confirm the theoretically computed Fermi surface, consisting of two electron-like and two hole-like and multiply degenerate sheets [9].

The low carrier density implies that each mobile electron is shared by several hundred formula units of $\text{Co}_3\text{Sn}_2\text{S}_2$. This distinct feature leads to an exceptionally large anomalous Hall angle [2]. Indeed, although the anomalous Hall conductivity of $\text{Co}_3\text{Sn}_2\text{S}_2$ ($\sigma_{xy}^A(2\text{K}) \simeq 1200(\Omega\text{cm})^{-1}$ [2, 8]) falls below what is seen in CoMn_2Ga ($\sigma_{xy}^A(2\text{K}) \simeq 2000(\Omega\text{cm})^{-1}$ [10]), the anomalous Hall angle attains a record magnitude ($\frac{\sigma_{xy}^A}{\sigma_{xx}}(120\text{K}) \simeq 0.2$) in $\text{Co}_3\text{Sn}_2\text{S}_2$ [2]. Another

consequence of high mobility is seen in the Nernst response. In contrast with low-mobility topological magnets (like Mn_3X ($\text{X}=\text{Sn}, \text{Ge}$) in which the Nernst effect is purely anomalous [11–13]), $\text{Co}_3\text{Sn}_2\text{S}_2$ has a sizeable ordinary Nernst response in addition to the anomalous component. Their ratio can be tuned by changing the concentration of impurities [8].

Together with Fe_3Sn_2 [14], $\text{Co}_3\text{Sn}_2\text{S}_2$ belongs to the restricted family of kagome ferromagnets. However, several recent experimental studies [15–26] suggested that the magnetic ordering in $\text{Co}_3\text{Sn}_2\text{S}_2$ is not purely ferromagnetic. In addition to the Curie temperature ($T_C \simeq 175$ K), there is an additional temperature scale, T_A . Muon spin-rotation (μSR) measurements [15] suggested the presence of an in-plane anti-ferromagnetic component emerging above 90 K that occupies an increasing volume fraction with warming and becomes dominant above 150 K. A Kerr microscopy study [17] reported that near $T_A \simeq 135$ K, domain wall mobility goes through a deep minimum, pointing to a phase transition within the domain walls. A recent neutron scattering study [18] found no evidence for antiferromagnetism in the magnetically ordered state and attributed the features observed near 125 K to a reduction of ferromagnetic domain size. Another study [19] found that an anti-ferromagnetic component emerges with indium doping in $\text{Co}_3\text{Sn}_2\text{S}_2$. Lachman *et al.* [21] found that the hysteresis loop of the anomalous Hall effect is not centered around zero field, a feature reminiscent of the so-called “exchange bias” effect in ferromagnet/antiferromagnet bilayers [27]. Moreover, they found that the magnetization hysteresis loop, which has a rectangular shape at low temperature, displays a “bow-tie” structure above

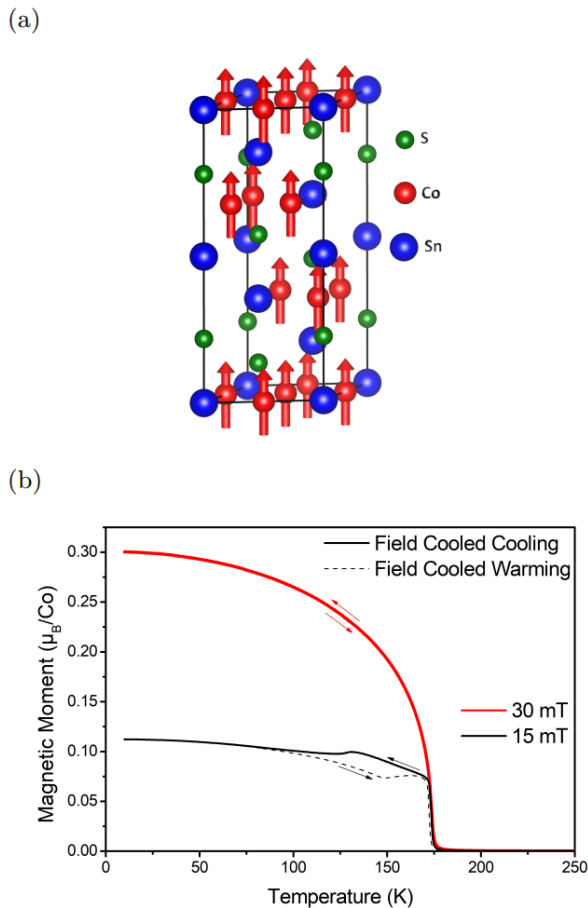


Figure 1: (a) Crystal structure of $\text{Co}_3\text{Sn}_2\text{S}_2$ with arrows showing the orientation of spins in the ordered phase. (b) Magnetization as a function of temperature at several magnetic fields. Above 22 mT, magnetization in the ferromagnetic phase is featureless. But when the sample is cooled down in presence of a magnetic field smaller than this threshold field, there is an anomaly and a hysteresis, which extends down to $\simeq 110$ K.

$T_A \simeq 125$ K. This led them to suggest the existence of a spin-glass phase. Zivkovic *et al.* [22] reported a similar change in the shape of the magnetic hysteresis loop and diagnosed a phase transition at $T_A \simeq 128$ K associated with a change in the canting angle of the magnetic moment away from the c -axis. On the other hand, Avakyants *et al.* [23], employing a First Order Reversal Curves (FORC) analysis, concluded that two independent magnetic phases coexist below T_C . Noah *et al.* [24] reported that the exchange bias found in this system [21] can be tuned by changing the prior history of the sample.

Here, we present a systematic study of magnetization as a function of temperature, magnetic field and prior magnetic history in $\text{Co}_3\text{Sn}_2\text{S}_2$ single crystals and identify the origin of T_A . We find that the “bow-tie” shape of the hysteresis loop [21, 25, 28] is not restricted to temperatures exceeding T_A . Even at low temperature, when the maximum field of opposite polarity visited by the sample (B_{max}) is sufficiently small, the hysteresis has a bow-tie shape [24]. Not only the shape

of the loop but also other features such as the threshold field for flipping spins (B_0) and the asymmetry between opposite field polarities ($B_{0+} \neq B_{0-}$), the exchange bias, depend on B_{max} . Thus, the system has a memory of the previously visited B_{max} . We identify a distinct small spin population as the driver of this memory. They keep their polarity even when the magnetic field is almost an order of magnitude larger than the coercive field for most ($> 99\%$) of the spin population. A detailed study of this memory effect leads us to conclude that T_A is not a thermodynamic phase transition, but a crossing point between boundaries in the (temperature, field) plane. One boundary separates memory-less and memory-full regimes. The other frontier determines the shape of the hysteresis loop and multiplicity of domains. When a single-domain state is abruptly replaced by a single-domain state of opposite polarity, the loop has a rectangular shape. A bow-tie shape emerges when the reversal has a multi-domain interlude. The existence of more than one type of ordered spins may be due to bulk/surface dichotomy [23]. Finally, by performing local magnetometry studied with miniature Hall probes, we show that when magnetization is not uniform, features associated with thermodynamics of small systems may emerge at length scales as large as a few microns.

II. Results

Figure 1b shows the temperature dependence of magnetization in one of our samples. Magnetization is enhanced below the Curie temperature of 175 K and saturates to 0.3 Bohr magneton, μ_B , per Co atom at low temperatures. Inside the ferromagnetic state, an anomaly and a hysteresis in temperature are detectable, which both disappear when the applied magnetic field becomes large enough to saturate magnetization.

A. Magnetization Hysteresis loops

Figure 2 a-f shows the evolution of the magnetization hysteresis loop as a function of temperature in a $\text{Co}_3\text{Sn}_2\text{S}_2$ single crystal. These loops were obtained by sweeping the field between -0.5 T and $+0.5$ T, corresponding to $B_{max} = 0.5$ T. At low temperatures (Fig 2 a,b,c), the hysteresis loop looks like a rectangle as in a hard magnet. The magnetic field suddenly flips all spins at well-defined thresholds identified as B_{0+} and B_{0-} . Let us define $B_0 = (B_{0+} - B_{0-})/2$, the average spin-flip field. At $T > 120$ K (Fig 2 d,e,f) the hysteresis loop is no more rectangular. This implies that all spins do not flip at $B = B_{0\pm}$. The jump in magnetization is followed by a smooth and almost field-linear variation of magnetization. This is the ‘bow-tie’ hysteresis shape [21].

The evolution seen in Figure 2 a-f is similar to what was reported by Lachman *et al.* [21], who found that the hysteresis loop acquires a ‘bow-tie’ shape above

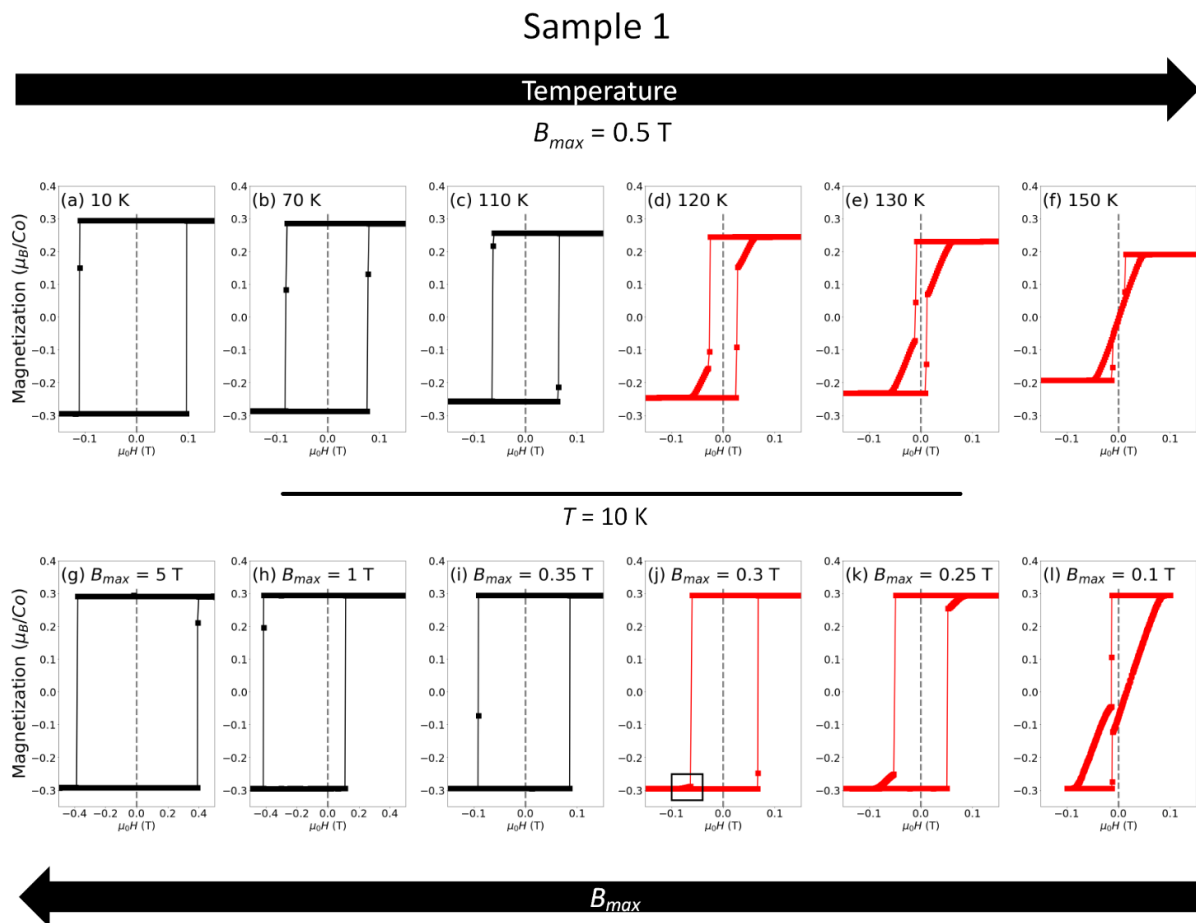


Figure 2: **Shape of the magnetization hysteresis loops** (a)-(f) Hysteresis loops at 10 K, 70 K, 110 K, 120 K, 130 K, 150 K, all with an identical maximum sweeping magnetic field ($B_{max} = 0.5 \text{ T}$). Note the emergence of a bow-tie feature above 120 K. (g)-(l) Hysteresis loops at $T = 10 \text{ K}$ with different maximums sweeping fields ($B_{max} = 5 \text{ T}$, 1 T , 0.35 T , 0.3 T , 0.25 T and 0.1 T). When B_{max} becomes smaller than 0.35 T , a bow-tie feature emerges.

a threshold temperature. The only difference is that our threshold temperature ($T_A = 115 \text{ K} \pm 5 \text{ K}$) is lower than theirs ($T_G = 125 \text{ K}$). This difference will be explained at the end of this paper. Another feature which appears at low temperature is a genuine asymmetry between positive and negative orientations: $B_{0+} \neq B_{0-}$ [21], which is particularly visible in Figure 2h.

Panels g-l in figure 2 show the hysteresis loops at 10 K with different maximum sweeping fields, B_{max} . The evolution is similar to the one induced by warming. When $B_{max} = 5 \text{ T}$, the magnetization loop is rectangular. Decreasing B_{max} reduces B_0 , in agreement with what was previously reported [24]. For sufficiently small B_{max} (that is, when $B_{max} < 0.35 \text{ T}$), the hysteresis loop acquires a bow-tie shape. The emergence of bow-tie shape and low values of B_0 are concomitant. We refer to the amplitude of B_0 below which the hysteresis loop displays a bow-tie feature as B_0^{bt} .

Thus, at low temperature, the shape of the hysteresis loop and the amplitude of B_0 both depend on B_{max} . In other words, the amplitude of magnetization at a

given magnetic field does not exclusively depend on temperature and magnetic field, but also on the magnetic field applied in the past. If the latter is not large enough, a memory persists. Memory formation in condensed matter is defined as an ‘ability to encode, access, and erase signatures of past history in the state of a system’ [29]. The present case is reminiscent of another topological magnet, namely Mn_3X (either with $\text{X}=\text{Sn}$ [30] or $\text{X}=\text{Ge}$ [31]). However, as we will see below, here the information is stocked not in the domain walls between antiferromagnetic domains, but in a secondary spin population.

B. Origin of the Bow-tie shape

Multiplicity of magnetic domains in $\text{Co}_3\text{Sn}_2\text{S}_2$, which occurs when the amplitude of magnetization is below its peak value of $M_s \simeq 0.3 \mu_B/\text{Co}$, has been probed by microscopic techniques [17, 32, 33]. To identify the origin of B_0^{bt} and the change in the shape of the hysteresis loop across this threshold, we scrutinized hysteresis loops with a very small ($< 0.2 \text{ T}$) B_{max} , leading to a magnetization lower than M_s .

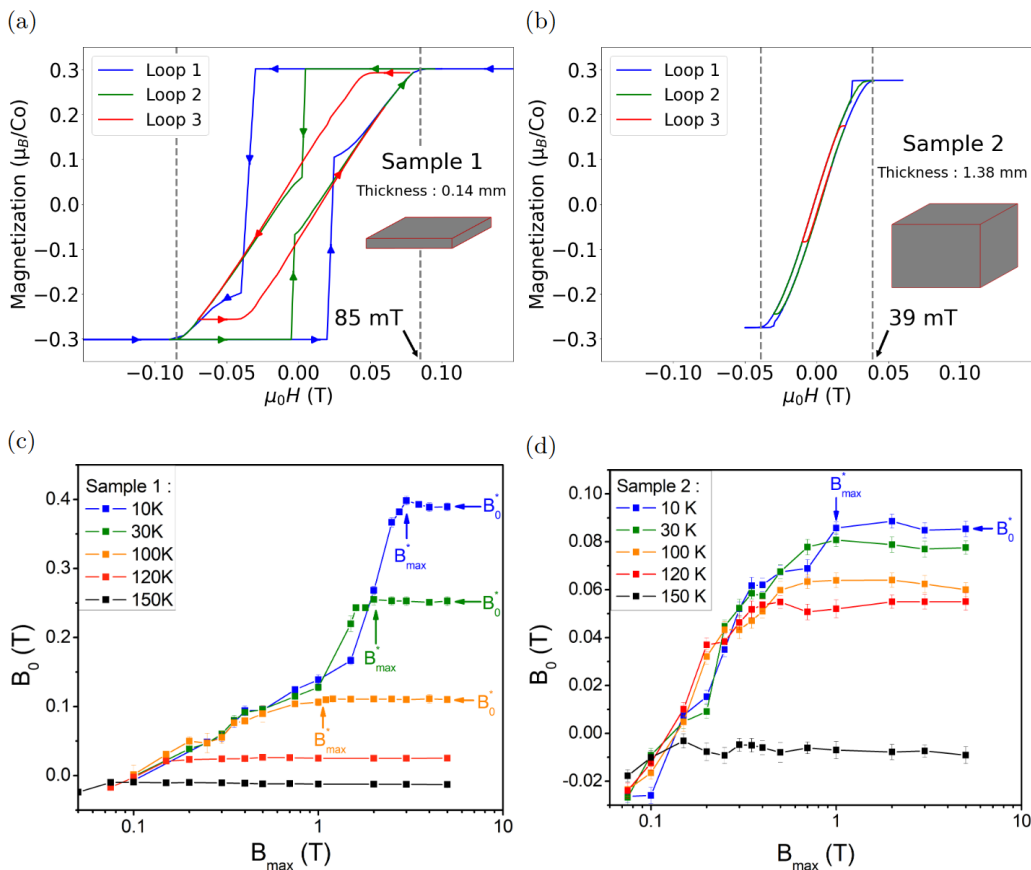


Figure 3: (a) Three Magnetization loops at 10 K. Loop 1 (blue): starting field at 0.2 T. Loop 2 (green): starting field at 0.1 T. Loop 3 (red): starting field at 0.08 T. (b) Loops for a thicker sample. Loop 1 (blue): starting field at 0.06 T. Loop 2 (green): starting field at 0.04 T. Loop 3 (red): starting field at 0.02 T. Bow-tie features tend to two parallel lines. (c) B_0 as function of B_{max} at different temperatures for sample 1; (d) Same for sample 2. At each temperature, B_0 initially increases linearly with increasing B_{max} . It eventually saturates to a constant value. This threshold sweeping field, B_{max}^* , is shown by arrows. The saturated amplitude of B_0 , called B_0^* is also shown. Both B_0^* and B_{max}^* decrease with increasing temperature.

Figure 3a illustrates the variation of magnetization with applied magnetic field during three successive hysteresis loops where the amplitude of B_{max} is incrementally reduced after each loop. The first two loops (blue and green) have a bow-tie shape: magnetization is first flat, then abruptly drops (or jumps) and then shows a steady drift towards its saturated value with a slope tending to be independent of B_{max} . During this steady drift, the system hosts multiple magnetic domains. In the third loop (red), B_{max} is so low that abrupt jumps (or drops) vanish. Note that the slope of magnetization in the red loop is similar to the slope of magnetization in the green and blue loops which presents a bow-tie shape. This slope, which does not depend on B_{max} , sets B_0^{bt} . Dividing $\mu_0 M_s$ by dM/dH yields 85 mT (Figure 3a), close to the threshold B_0^{bt} revealed in the transition between panels i and j of Figure 2.

Magnetization loops for a thicker sample (Figure 3b) are similar, but there is a quantitative difference. The magnetization slope is steeper in the thicker sample, which has almost a cubic shape. M_s is identical in the two samples and therefore the threshold field is re-

duced to 39 mT in this thicker sample. Thus, with increasing thickness, the multi-domain window becomes narrower, the magnetization slope becomes steeper and B_0^{bt} is reduced.

The difference in the demagnetizing factors of the two samples provides a quantitative account of this thickness dependence. As seen in table I, D , the demagnetizing factor calculated by using the formula for a rectangular prism [34], is very close to $\frac{dH}{dM}$, the inverse of the magnetization slope measured in the experiment.

When the magnetic field becomes equal to $B_{0\pm}$, an energy barrier is crossed and spins flip to the opposite orientation. If $|B_{0\pm}| \geq \mu_0 DM_s$, the spin-flip is total and the loop is rectangular. On the other hand, if $|B_{0\pm}| \leq \mu_0 DM_s$, spin-flip is partial and the loop has a bow-tie shape, because a multi-domain configuration is stable thanks to the demagnetization energy. This leads us to $B_0^{bt} = \mu_0 DM_s$, in agreement with the experimental observation.

	Dimensions (mm^3)	Aspect ratio	D	dH/dM
Sample 1	$1.21 \times 0.89 \times 0.14$	0.13	0.76	0.69
Sample 2	$1.93 \times 1.20 \times 1.38$	0.88	0.35	0.38

Table I: Samples dimensions and aspect ratio. For both samples, the calculated demagnetizing factor, D , is close to the measured dH/dM (the inverse of the magnetization slope) when $B < B_0^{bt}$ implying $B_0^{bt} = \mu_0 D M_s$.

C. Temperature dependence of the memory effect

We saw that the magnitude of B_0 depends on the maximum sweeping field, B_{max} . Figure 3c illustrates this dependence for different temperatures in a semi-log plot. At each temperature, the initial increase B_0 , which is roughly linear in B_{max} ends by saturation to a constant value, which we dub B_0^* . Let us call B_{max}^* the magnitude of B_{max} above which $B_0 = B_0^*$. As one can see in the figure, both B_0^* and B_{max}^* steadily decrease with increasing temperature. The picture drawn by this data is following: when $B_{max} < B_{max}^*$, the system has a memory, which shows itself in the magnitude of B_0 . Spin flip occurs at a threshold magnetic field, which depends on the previously visited field. When $B_{max} > B_{max}^*$, there is no such memory and $B_0(T) = B_0^*(T)$ is independent of previous history.

Figure 3d presents the same data for the thicker sample (#2). The behavior is qualitatively similar: After an initial increase, B_0 saturates at a temperature dependent magnitude. Note, however, that the absolute value of B_0^* is much smaller in the thicker sample. At low temperature, $B_0^* \simeq 0.4$ T in sample 1 and $B_0^* \simeq 0.09$ T in sample 2. It is noteworthy that, for both samples, $B_{max}^*/B_0^* \approx 8$ and this ratio does not show any strong temperature dependence. This indicates that the temperature-induced decrease in both field scales is similar.

B_0^* is the coercive field of the system when the memory is erased. As expected [35], it decreases with increasing temperature. Its amplitude in the zero-temperature limit is much smaller than the magnetocrystalline anisotropy field, i.e. to the in-plane magnetic field needed to saturate magnetization. The latter is as large as ~ 23 T [36]. This difference makes $Co_3Sn_2S_2$ another example of what is known as 'Brown's coercivity paradox' [37]. Experiments have found that the coercivity is often much smaller than the lowest bound expected according to the magnetocrystalline anisotropy [38]. It has been shown that large demagnetizing fields developed near sharp corners play a significant role in setting coercivity [37] and imperfections can reduce the expected coercive field [39].

Thus, when the maximum sweeping field B_{max} becomes lower than a threshold (B_{max}^*), B_0 becomes lower than its peak value $B_0^* \simeq 0.4$ T. Moreover, this is also the case of the difference between $|B_{0+}|$ and $|B_{0-}|$, which becomes significantly larger than our experimental margin. Thus, the memory effect tunes the exchange bias, too (See the Supplementary Materials

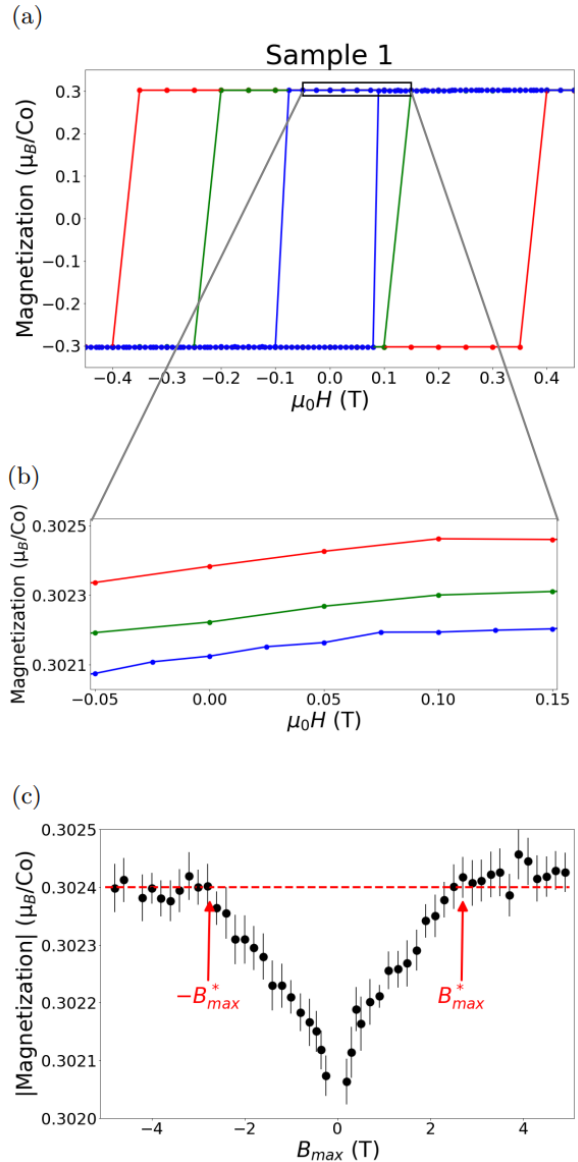


Figure 4: Memory effect in "saturated" magnetization, at 10 K. (a) Three magnetization loops, red : $B_{max} = 4.8$ T, green: $B_{max} = 1.5$ T and blue: $B_{max} = 0.5$ T. (b) Zoom in positive magnetization at low field. (c) B_{max} dependence of the absolute value of magnetization at ± 50 mT (depending on B_{max} sign).

for details [40]).

D. Zooming on saturated magnetization

Given the content of this memory, one may suspect that when it is not erased, the energy barrier between

two single-domain states is attenuated. This may be caused by the presence of a secondary spin component or population which modifies the overall energy landscape and attenuates the height of the barrier. A careful examination of saturated magnetization at the end of a hysteresis loop confirms this.

Figure 4a displays three loops all at 10 K with three different endings ($B_{max}=0.5$ T; 1.5 T and 4.8 T). The figure shows that B_0 increases with increasing B_{max} , as we saw above. At first sight, magnetization appears to saturate at the same amplitude. However, this is not the case. Figure 4b is a zoom on the three curves near the maximum magnetization. One can see that there is a small, yet finite difference between the three curves. With increasing B_{max} , the amplitude of magnetization at the end of a ‘rectangular’ loop is larger. We carefully documented the dependence of spontaneous magnetization at the end of a loop (measured at $B = \pm 0.05$ T) on the amplitude of the sweeping magnetic field.

Figure 4c shows the result. The spontaneous magnetization at the end of a loop increases with increasing $|B_{max}|$ before saturating to a constant value when B_{max} becomes equal to B_{max}^* . The detected increase of magnetization between B_0^* (the end of the loop) and its eventual saturation above B_{max}^* is tiny ($\approx 0.1\%$), but larger than our experimental margin. This observation has an important implication: when the sample has not visited a sufficiently large B_{max} , it hosts a small population of spins whose magnetization does not correspond to the polarity of majority spins. This population is where the memory is stored. The existence of a B_{max}^* (roughly 8 times larger than B_0^*) is caused by this secondary spin population whose coercive field is larger and much more broadly distributed than the coercive field of the majority spins. The secondary spins, presumably three orders of magnitude more dilute than the principal population, may be situated either at the surface of the sample or at off-stoichiometric sites.

III. Discussion

Having identified four different field scales (See table II), let us now turn our attention to the phase diagram.

A. Origin of T_A , the additional temperature scale

Figure 5a shows the evolution of B_0^* and B_0^{bt} with temperature. B_0^{bt} , the threshold field for bow-tie shape, is almost flat and its absolute value coincides with $\mu_0 DM_s$. In contrast, B_0^* , the saturated B_0 , is temperature dependent and rapidly decreases with increasing temperature. T_A is the temperature at which B_0^* and B_0^{bt} cross each other. When B_0^* falls below B_0^{bt} , whatever the sweeping field B_{max} , one finds $B_0 < B_0^{bt}$.

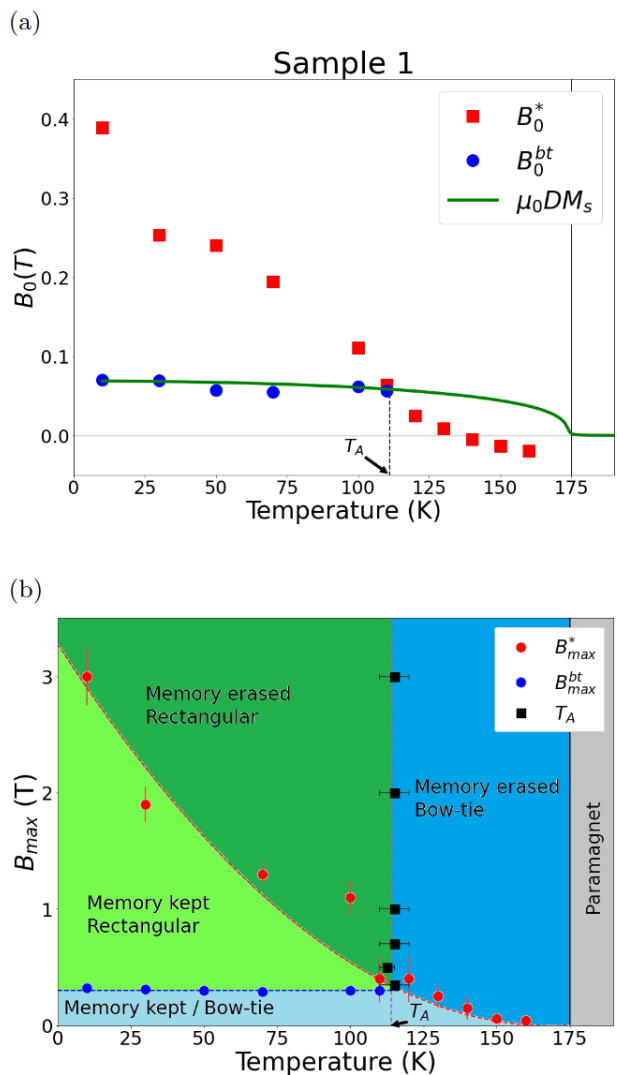


Figure 5: (a) B_0^* and B_0^{bt} versus temperature. The measured B_0^{bt} tracks $\mu_0 DM_s$ (with $D = 0.76$), which is represented by the green solid line. B_0^* and B_0^{bt} cross each other at T_A . Above this, hysteresis loops can only have a bow-tie shape for whatever B_{max} , because of the $B_0^* < B_0^{bt}$ inequality. (b) B_{max}^* and B_{max}^{bt} versus temperature. Dashed lines are guides to the eye. $T_A = 115 \pm 5$ K, corresponds to the crossing point of B_{max}^* and B_{max}^{bt} .

This makes a bow-tie shape unavoidable. Thus, no thermodynamic phase transition occurs at T_A . This temperature threshold arises as a result of the crossing between two boundaries.

This is further illustrated in Figure 5b, a representation of the evolution of B_{max}^* and B_{max}^{bt} in the (field, temperature) plane. When $B_{max} > B_{max}^*$, the system has no memory (that is, the shape of hysteresis loop does not depend on the past history) and when $B_{max} < B_{max}^*$, there is a memory. $B_{max}^*(T)$ is the boundary between two states with and without memory. A second boundary is defined by B_{max}^{bt} . When B_{max} is larger than this threshold, the hysteresis loop is rectangular. Since B_{max}/B_0 ratio does not change with temperature, T_A , the temperature at

Field scale	Amplitude (T)	Definition
B_0^* (T)	0.4	Spin-flip field in absence of memory (coercivity of main spin population)
B_{max}^* (T)	3	Sweeping field above which no memory persists (maximum coercivity of secondary spin population)
B_0^{bt} (T)	0.085	Hysteresis becomes bow-tie when the spin-flip field falls below this threshold
B_{max}^{bt} (T)	0.35	Hysteresis becomes bow-tie when the magnetic field is swept below this threshold

Table II: Four distinct field scales identified in this study. The amplitudes are given for sample 1 at $T = 10$ K. B_0^* and B_0^{bt} refer to spin-flip fields, at which the magnetic field shows an abrupt jump. B_{max}^{bt} and B_{max}^* refer to maximum sweeping field tuning the spin-flip field, B_0 . B_0^{bt} and B_{max}^{bt} depend on the demagnetizing factor and show little dependence on temperature. B_{max}^* and B_0^* both decrease with warming.

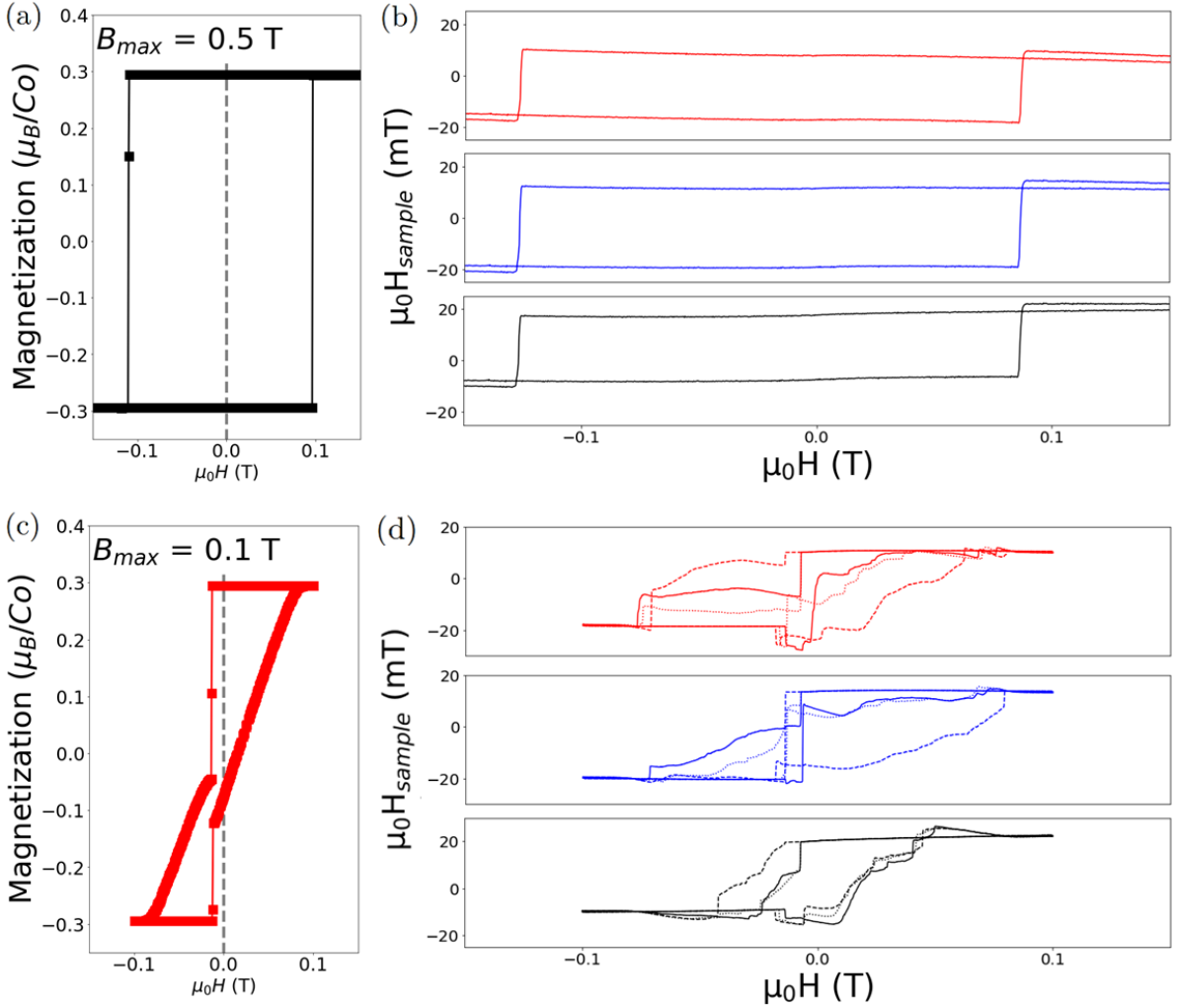


Figure 6: Local and global magnetization. (a) Magnetization of the whole sample, measured with a vibrating-sample magnetometer, at 10 K for $B_{max} = 0.5$ T. (b) Local magnetization, measured in identical conditions by an array of 2DEG micron-sizes Hall sensors put on the surface of the sample. The three curves represent the local magnetic field at three different positions of the sample. (c) Magnetization of the whole sample at 10 K for $B_{max} = 0.1$ T. Hysteresis displays a bow-tie shape. (d) Local magnetization measured in similar conditions. Each color represents a position on the sample (three consecutive hysteresis loops were measured.)

which $B_{max}^{bt} = B_{max}^*$ is similar to what can be seen in Figure 5a. Since B_0^{bt} and B_{max}^{bt} depend on the demagnetizing factor and the sample morphology, the horizontal lines in these figures are expected to vary from sample to sample with the change in the aspect ratio. This would explain the fact that the reported secondary temperature differs from one study to another.

Thus, the magnetic order in $\text{Co}_3\text{Sn}_2\text{S}_2$ remains ferromagnetic with spins oriented along the c-axis. However, in presence of a magnetic field oriented along the c-axis, as a function of temperature and magnetic field (both at present and in the past), multiple meta-stable configurations can arise. What distinguishes them is the polarity in different sub-sets of spin population, despite the global ferromagnetic order.

B. Thermodynamic limit for well-defined magnetization

One manifestation of this meta-stability is the contrast between local and global magnetization, shown in Figure 6. When the system is in the rectangular regime, local magnetization, measured with micron-sized Hall sensors (see supplementary material for details [40]), is very similar to the magnetization of the whole sample. In other words, the passage between single-domain regimes of opposite polarities is almost identical everywhere in the sample (Figure 6 a & b). On the other hand, when the sample is multi-domain, while global magnetization presents a smooth and reproducible slope (Figure 6c), local magnetization is not reproducible from one sweep to another (Figure 6d). This confirms that when the memory is not erased, the energy landscape is not smooth [41]. There are numerous competing spin configurations, spatially distinct over a micrometer, but with similar global magnetization. Our case emerges as a platform for studying thermodynamics of small systems [42].

C. Possibly related phenomena in other magnetic solids

Let us note that $\text{Co}_3\text{Sn}_2\text{S}_2$ is not the first case of multiple spin populations. In SrRuO_3 thin films [43, 44] with a thickness of few unit cells, there is an additional peak in the Hall response. It has been proposed that it is caused by contributions of opposite signs from two distinct magnetic regions with different saturation magnetizations [45]. The two contributions have different coercive fields, but this difference is far below the order of magnitude difference we see in our case. A similar observation has been reported in NiCo_2O_3 thin films [46].

These observations indicate that the existence of distinct spin populations with different coercive fields in a magnet may be more common than previously thought.

IV. Conclusion

In summary, we investigated the evolution of the magnetization hysteresis loop in $\text{Co}_3\text{Sn}_2\text{S}_2$ with temperature and with the maximum swept magnetic field, B_{max} . We found that, at each temperature, increasing B_{max} leads to an enhancement of the coercive field up to a saturation value, B_{max}^* . In addition, the amplitude of the saturated magnetization displays a small, yet significant, dependence on B_{max} . This suggests the presence of a small secondary spin population with a coercive field larger than that of the main population. The memory of the last B_{max} is stored by this minority spins, which do not flip if the sweeping field is lower than B_{max}^* .

A temperature scale, T_A , distinct from the Curie tem-

perature, was identified by several previous studies. It was suggested that it corresponds to a thermodynamic phase transition within the magnetically ordered state. This secondary phase was suggested to be in-plane antiferromagnetism [15], spin glass [21] or an anomaly in domain wall mobility [17]. According to our study, T_A does not correspond to a thermodynamic phase transition, but to a crossing point between meta-stable states. The two boundaries which cross at T_A separate regimes with and without memory and regimes which are single-domain and multiple-domain. The origin of the two distinct coercive fields corresponding to two distinct spin populations emerges as a puzzle to be addressed by future studies.

V. Acknowledgements

This study was supported by Jeunes Equipes de l'Institut de Physique du Collège de France, and by a grant attributed by the Ile de France regional council. C. M. acknowledges a PhD scholarship granted by CNRS.

VI. Methods

Crystals of $\text{Co}_3\text{Sn}_2\text{S}_2$ were grown by self-flux method as detailed previously [9].

Magnetization was measured using a Quantum Design MPMS in Vibrating Sample Magnetometer (VSM) mode with magnetic field applied along the crystalline c-axis with a quartz sample holder.

The hysteresis loops displayed in figures 2 and 3 c-d, were obtained according to the following protocol :

- Set the temperature.
- Reduce the remanent field by sweeping the applied field with gradually decreasing $|B_{max}|$ until finding that magnetization is not saturated anymore. For instance, the field was swept first from -0.5 T, to 0.2 T then to -0.1 T, then to 0.05 T, and finally to 0 T.
- Loops were measured consecutively, starting from the smallest to the largest B_{max} without additional delay between steps of measurement.
- Loops measurement were done by initially setting the external field to B_{max} (with a sweep rate of 100 Oe/s). Then the external field was swept at 10 Oe/s in linear mode from B_{max} to $-B_{max}$, then swept back to B_{max} .

Loops in figure 4 were obtained by decreasing B_{max} . They are similar to experiments performed by increasing B_{max} .

To measure local magnetization, we employed an array of Hall sensors based on high-mobility AlGaAs/GaAs heterostructure with a 160 nm two-

dimensional electron gas (2DEG) below the surface, as done before [30, 47, 48]. The device was fabricated using electron beam lithography and 250 V argon ions to define the mesa. The device consists of ten $5 \times 5 \mu\text{m}^2$ sensors separated from their neighbor by $100 \mu\text{m}$. The

hall resistance of the sensors are $R_{Hall} \approx 6.2 \times 10^3 * B$. The local magnetic field at the surface of the sample was obtained by measuring the Hall resistivity of a sensor put on the sample. The sensor resistivity was measured using a Quantum Design PPMS with applied field along the c-axis of the sample.

-
- [1] M. Zabel, S. Wandering, and K.-J. Range, Ternary Chalcogenides $M_3M_2X_2$ with Shandite-Type Structure, *Zeitschrift für Naturforschung B* **34**, 238 (1979).
- [2] E. Liu, Y. Sun, N. Kumar, L. Muechler, A. Sun, L. Jiao, S.-Y. Yang, D. Liu, A. Liang, Q. Xu, *et al.*, Giant anomalous Hall effect in a ferromagnetic kagome-lattice semimetal, *Nature physics* **14**, 1125 (2018).
- [3] Q. Wang, Y. Xu, R. Lou, Z. Liu, M. Li, Y. Huang, D. Shen, H. Weng, S. Wang, and H. Lei, Large intrinsic anomalous Hall effect in half-metallic ferromagnet $\text{Co}_3\text{Sn}_2\text{S}_2$ with magnetic Weyl fermions, *Nature communications* **9**, 3681 (2018).
- [4] P. Vaqueiro and G. G. Sobany, A powder neutron diffraction study of the metallic ferromagnet $\text{Co}_3\text{Sn}_2\text{S}_2$, *Solid State Sciences* **11**, 513 (2009).
- [5] Y. S. Dedkov, M. Holder, S. L. Molodtsov, and H. Rosner, Electronic structure of shandite $\text{Co}_3\text{Sn}_2\text{S}_2$, *Journal of Physics: Conference Series* **100**, 072011 (2008).
- [6] M. Holder, Y. S. Dedkov, A. Kade, H. Rosner, W. Schnelle, A. Leithe-Jasper, R. Wehrich, and S. L. Molodtsov, Photoemission study of electronic structure of the half-metallic ferromagnet $\text{Co}_3\text{Sn}_2\text{S}_2$, *Phys. Rev. B* **79**, 205116 (2009).
- [7] W. Schnelle, A. Leithe-Jasper, H. Rosner, F. M. Schappacher, R. Pöttgen, F. Pielhofer, and R. Wehrich, Ferromagnetic ordering and half-metallic state of $\text{Sn}_2\text{Co}_3\text{S}_2$ with the shandite-type structure, *Phys. Rev. B* **88**, 144404 (2013).
- [8] L. Ding, J. Koo, L. Xu, X. Li, X. Lu, L. Zhao, Q. Wang, Q. Yin, H. Lei, B. Yan, *et al.*, Intrinsic anomalous Nernst effect amplified by disorder in a half-metallic semimetal, *Physical Review X* **9**, 041061 (2019).
- [9] L. Ding, J. Koo, C. Yi, L. Xu, H. Zuo, M. Yang, Y. Shi, B. Yan, K. Behnia, and Z. Zhu, Quantum oscillations, magnetic breakdown and thermal Hall effect in $\text{Co}_3\text{Sn}_2\text{S}_2$, *Journal of Physics D: Applied Physics* **54**, 454003 (2021).
- [10] A. Sakai, Y. P. Mizuta, A. A. Nugroho, R. Sishombing, T. Koretsune, M.-T. Suzuki, N. Takemori, R. Ishii, D. Nishio-Hamane, R. Arita, P. Goswami, and S. Nakatsuji, Giant anomalous Nernst effect and quantum-critical scaling in a ferromagnetic semimetal, *Nature Physics* **14**, 1119 (2018).
- [11] X. Li, L. Xu, L. Ding, J. Wang, M. Shen, X. Lu, Z. Zhu, and K. Behnia, Anomalous Nernst and Righi-Leduc effects in Mn_3Sn : Berry curvature and entropy flow, *Phys. Rev. Lett.* **119**, 056601 (2017).
- [12] M. Ikhlas, T. Tomita, T. Koretsune, M.-T. Suzuki, D. Nishio-Hamane, R. Arita, Y. Otani, and S. Nakatsuji, Large anomalous Nernst effect at room temperature in a chiral antiferromagnet, *Nature Physics* **13**, 1085 (2017).
- [13] L. Xu, X. Li, X. Lu, C. Collignon, H. Fu, J. Koo, B. Fauqué, B. Yan, Z. Zhu, and K. Behnia, Finite-temperature violation of the anomalous transverse Wiedemann-Franz law, *Science Advances* **6**, eaaz3522 (2020).
- [14] Z. Ren, H. Li, S. Sharma, D. Bhattarai, H. Zhao, B. Rachmilowitz, F. Bahrami, F. Tafti, S. Fang, M. P. Ghimire, Z. Wang, and I. Zeljkovic, Plethora of tunable weyl fermions in kagome magnet Fe_3Sn_2 thin films, *npj Quantum Materials* **7**, 109 (2022).
- [15] Z. Guguchia, J. Verezhak, D. Gawryluk, S. Tsirkin, J.-X. Yin, I. Belopolski, H. Zhou, G. Simutis, S.-S. Zhang, T. Cochran, *et al.*, Tunable anomalous hall conductivity through volume-wise magnetic competition in a topological kagome magnet, *Nature communications* **11**, 559 (2020).
- [16] Q. Zhang, S. Okamoto, G. D. Samolyuk, M. B. Stone, A. I. Kolesnikov, R. Xue, J. Yan, M. A. McGuire, D. Mandrus, and D. A. Tennant, Unusual Exchange Couplings and Intermediate Temperature Weyl State in $\text{Co}_3\text{Sn}_2\text{S}_2$, *Physical Review Letters* **127**, 117201 (2021).
- [17] C. Lee, P. Vir, K. Manna, C. Shekhar, J. Moore, M. Kastner, C. Felser, and J. Orenstein, Observation of a phase transition within the domain walls of ferromagnetic $\text{Co}_3\text{Sn}_2\text{S}_2$, *Nature communications* **13**, 3000 (2022).
- [18] J.-R. Soh, C. Yi, I. Zivkovic, N. Qureshi, A. Stunault, B. Ouladdiaf, J. A. Rodríguez-Velamazán, Y. Shi, H. M. Rønnow, and A. T. Boothroyd, Magnetic structure of the topological semimetal $\text{Co}_3\text{Sn}_2\text{S}_2$, *Physical Review B* **105**, 094435 (2022).
- [19] K. J. Neubauer, F. Ye, Y. Shi, P. Malinowski, B. Gao, K. M. Taddei, P. Bourges, A. Ivanov, J.-H. Chu, and P. Dai, Spin structure and dynamics of the topological semimetal $\text{Co}_3\text{Sn}_{2-x}\text{In}_x\text{S}_2$, *npj Quantum Materials* **7**, 112 (2022).
- [20] M. A. Kassem, Y. Tabata, T. Waki, and H. Nakamura, Low-field anomalous magnetic phase in the kagome-lattice shandite $\text{Co}_3\text{Sn}_2\text{S}_2$, *Physical Review B* **96**, 014429 (2017).
- [21] E. Lachman, R. A. Murphy, N. Maksimovic, R. Kealhofer, S. Haley, R. D. McDonald, J. R. Long, and J. G. Analytis, Exchange biased anomalous Hall effect driven by frustration in a magnetic kagome lattice, *Nature communications* **11**, 560 (2020).
- [22] I. Živković, R. Yadav, J.-R. Soh, C. Yi, Y. Shi, O. V. Yazyev, and H. M. Rønnow, Unraveling the origin of the peculiar transition in the magnetically ordered phase of the Weyl semimetal $\text{Co}_3\text{Sn}_2\text{S}_2$, *Physical Review B* **106**, L180403 (2022).
- [23] A. Avakyants, N. Orlova, A. Timonina, N. Kolesnikov, and E. Deviatov, Evidence for surface spin structures from first order reversal curves in $\text{Co}_3\text{Sn}_2\text{S}_2$ and Fe_3GeTe_2 magnetic topological semimetals, *Journal of Magnetism and Magnetic Materials* **573**, 170668 (2023).
- [24] A. Noah, F. Toric, T. D. Feld, G. Zissman, A. Gutfreund, D. Tsruya, T. Devidas, H. Alpern, A. Vakahi,

- H. Steinberg, *et al.*, Tunable exchange bias in the magnetic Weyl semimetal $\text{Co}_3\text{Sn}_2\text{S}_2$, *Physical Review B* **105**, 144423 (2022).
- [25] Z. Shen, X. Zhu, R. R. Ullah, P. Klavins, and V. Taufour, Anomalous depinning of magnetic domain walls within the ferromagnetic phase of the Weyl semimetal $\text{Co}_3\text{Sn}_2\text{S}_2$, *Journal of Physics: Condensed Matter* **35**, 045802 (2022).
- [26] Q. Zhang, Y. Zhang, M. Matsuda, V. O. Garlea, J. Yan, M. A. McGuire, D. A. Tennant, and S. Okamoto, Hidden local symmetry breaking in a kagome-lattice magnetic Weyl semimetal, *Journal of the American Chemical Society* **144**, 14339 (2022).
- [27] R. L. Stamps, Mechanisms for exchange bias, *Journal of Physics D: Applied Physics* **33**, R247 (2000).
- [28] S. E. Pate, B. Wang, B. Shen, J. S. Jiang, U. Welp, W.-K. Kwok, J. Xu, K. Li, R. Divan, and Z.-L. Xiao, Field orientation dependent magnetic phases in the weyl semimetal $\text{Co}_3\text{Sn}_2\text{S}_2$, *Physical Review B* **108**, L100408 (2023).
- [29] N. C. Keim, J. D. Paulsen, Z. Zeravcic, S. Sastry, and S. R. Nagel, Memory formation in matter, *Rev. Mod. Phys.* **91**, 035002 (2019).
- [30] X. Li, C. Collignon, L. Xu, H. Zuo, A. Cavanna, U. Gennser, D. Maily, B. Fauqué, L. Balents, Z. Zhu, *et al.*, Chiral domain walls of Mn_3Sn and their memory, *Nature communications* **10**, 3021 (2019).
- [31] L. Xu, X. Li, L. Ding, K. Behnia, and Z. Zhu, Planar Hall effect caused by the memory of antiferromagnetic domain walls in Mn_3Ge , *Applied Physics Letters* **117**, 222403 (2020).
- [32] A. Sugawara, T. Akashi, M. A. Kassem, Y. Tabata, T. Waki, and H. Nakamura, Magnetic domain structure within half-metallic ferromagnetic kagome compound $\text{Co}_3\text{Sn}_2\text{S}_2$, *Physical Review Materials* **3**, 104421 (2019).
- [33] S. Howlader, R. Ramachandran, Y. Singh, G. Sheet, *et al.*, Domain structure evolution in the ferromagnetic Kagome-lattice Weyl semimetal $\text{Co}_3\text{Sn}_2\text{S}_2$, *Journal of Physics: Condensed Matter* **33**, 075801 (2020).
- [34] A. Aharoni, Demagnetizing factors for rectangular ferromagnetic prisms, *Journal of applied physics* **83**, 3432 (1998).
- [35] J. Garcia-Otero, A. Garcia-Bastida, and J. Rivas, Influence of temperature on the coercive field of non-interacting fine magnetic particles, *Journal of magnetism and magnetic materials* **189**, 377 (1998).
- [36] J. Shen, Q. Zeng, S. Zhang, W. Tong, L. Ling, C. Xi, Z. Wang, E. Liu, W. Wang, G. Wu, *et al.*, On the anisotropies of magnetization and electronic transport of magnetic Weyl semimetal $\text{Co}_3\text{Sn}_2\text{S}_2$, *Applied Physics Letters* **115** (2019).
- [37] U. Hartmann, Origin of Brown's coercive paradox in perfect ferromagnetic crystals, *Physical Review B* **36**, 2331 (1987).
- [38] J. M. Coey, *Magnetism and magnetic materials* (Cambridge university press, 2010) p. 245.
- [39] A. Aharoni, Reduction in coercive force caused by a certain type of imperfection, *Physical Review* **119**, 127 (1960).
- [40] See Supplemental Material for more details (2024).
- [41] D. J. Wales, Energy landscapes, in *Atomic clusters and nanoparticles. Agregats atomiques et nanoparticules: Les Houches Session LXXIII 2-28 July 2000*, edited by C. Guet, P. Hobza, F. Spiegelman, and F. David (Springer Berlin Heidelberg, Berlin, Heidelberg, 2001) pp. 437-507.
- [42] T. Hill, *Thermodynamics of Small Systems*, Dover Books on Chemistry (Dover Publications, 1994).
- [43] Z. Ding, X. Chen, Z. Wang, Q. Zhang, F. Yang, J. Bi, T. Lin, Z. Wang, X. Wu, M. Gu, M. Meng, Y. Cao, L. Gu, J. Zhang, Z. Zhong, X. Liu, and J. Guo, Magnetism and berry phase manipulation in an emergent structure of perovskite ruthenate by (111) strain engineering, *npj Quantum Materials* **8**, 43 (2023).
- [44] U. Kar, A. K. Singh, Y.-T. Hsu, C.-Y. Lin, B. Das, C.-T. Cheng, M. Berben, S. Yang, C.-Y. Lin, C.-H. Hsu, S. Wiedmann, W.-C. Lee, and W.-L. Lee, The thickness dependence of quantum oscillations in ferromagnetic Weyl metal SrRuO_3 , *npj Quantum Materials* **8**, 8 (2023).
- [45] G. Kimbell, P. M. Sass, B. Woltjes, E. K. Ko, T. W. Noh, W. Wu, and J. W. Robinson, Two-channel anomalous Hall effect in SrRuO_3 , *Physical Review Materials* **4**, 054414 (2020).
- [46] G. Zhou, P. Kang, H. Ji, J. Dou, S. Wang, and X. Xu, Observation of two-channel anomalous Hall effect in perpendicularly magnetized NiCo_2O_4 epitaxial films, *Physical Review B* **108**, 094442 (2023).
- [47] C. Collignon, B. Fauqué, A. Cavanna, U. Gennser, D. Maily, and K. Behnia, Superfluid density and carrier concentration across a superconducting dome: The case of strontium titanate, *Phys. Rev. B* **96**, 224506 (2017).
- [48] K. Behnia, C. Capan, D. Maily, and B. Etienne, Internal avalanches in a pile of superconducting vortices, *Phys. Rev. B* **61**, R3815 (2000).

Supplementary Materials for "Magnetic memory and distinct spin populations in ferromagnetic $\text{Co}_3\text{Sn}_2\text{S}_2$ "

Supplementary note 1. Samples

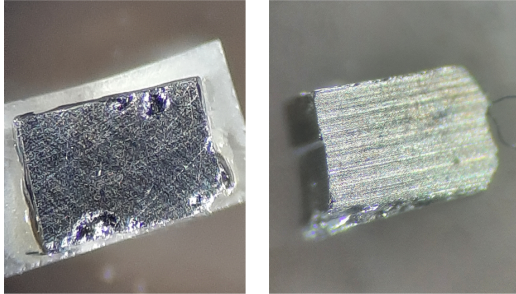


Figure Supplementary 1: Picture of $\text{Co}_3\text{Sn}_2\text{S}_2$ samples. (left) Sample 1, (right) Sample 2.

Supplementary figure 1 shows pictures of $\text{Co}_3\text{Sn}_2\text{S}_2$ crystals used in this study. Sample dimensions are $1.21 \times 0.89 \times 0.14 \text{ mm}^3$ for sample 1 and $1.93 \times 1.20 \times 1.38 \text{ mm}^3$ for sample 2.

Supplementary note 2. Resistivity data

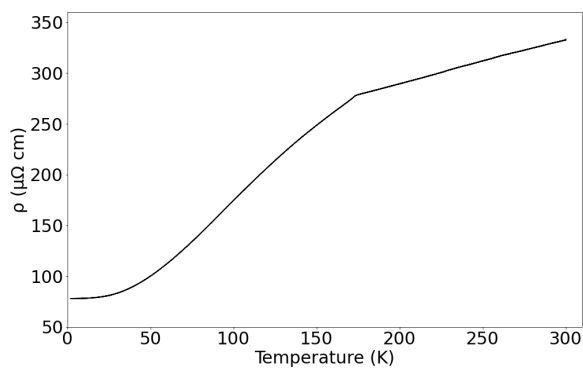


Figure Supplementary 2: Resistivity of sample 1 versus temperature at zero field.

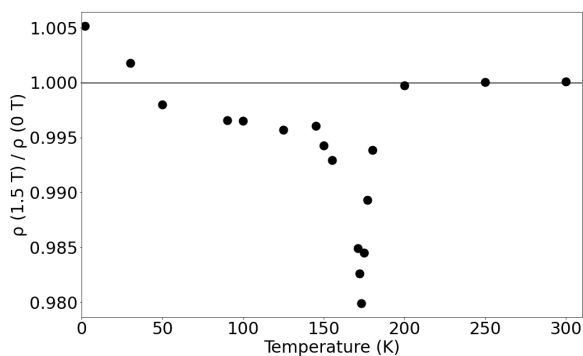


Figure Supplementary 3: Resistivity at 1.5 T normalized by resistivity at zero field as a function of temperature.

Supplementary figure 2 displays resistivity of sample 1 versus temperature. We observe a kink at 173 K, corresponding to the ferromagnetic-paramagnetic transition at Curie temperature T_C .

Supplementary figure 3 displays resistivity under an applied field of 1.5 T normalised by resistivity at zero field. There is a minimum around 173 K, which also correspond to T_C .

Supplementary note 3. Magnetization measurements

Performing multiple loops with increasing B_{max} causes B_0 to increase with some steps, which may vary between measurements. Supplementary figure 4 compares B_{0+} measurement for increasing and decreasing B_{max} . There is no significant difference between increasing and decreasing B_{max} . Both protocols gave similar results.

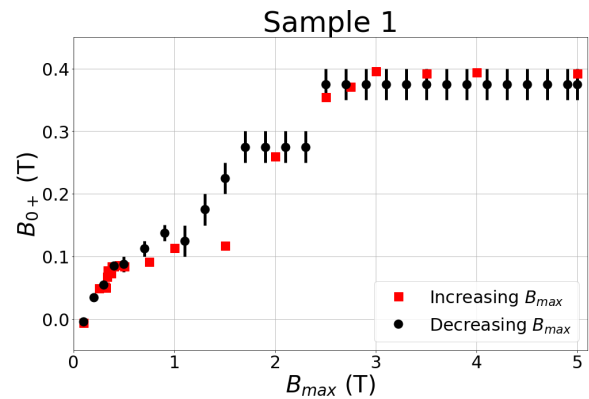


Figure Supplementary 4: Positive spin flip field (B_{0+}) for increasing and decreasing B_{max} .

Supplementary note 4. Exchange Bias

The exchange bias field, defined as $B_{EB} = (|B_{0+}| - |B_{0-}|)/2$ depends on B_{max} too. Supplementary figure 5 shows B_{EB} at 10 K, 30 K and 100 K. The amplitude of B_{EB} was found to strongly fluctuates and its sign differs between successive hysteresis loops. However, when $B_{max} > B_{max}^*$, the amplitude of B_{EB} becomes as small as the statistical error margin.

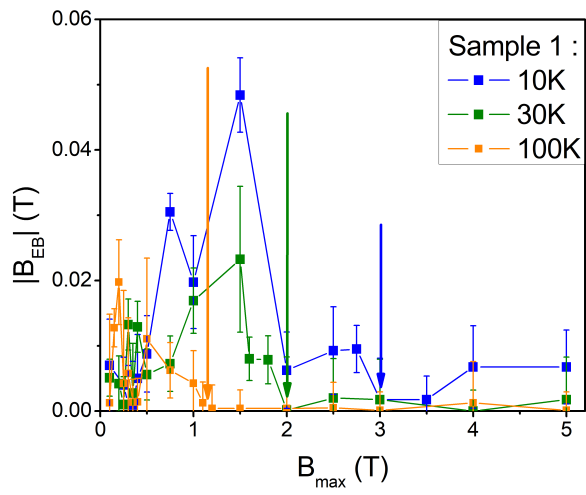


Figure Supplementary 5: Exchange bias field, $|B_{EB}|$ as a function of B_{max} at several temperatures.

Supplementary note 5. Local magnetization

Supplementary figure 6 is a picture of the arrays of Hall sensors used to measure local magnetization of our samples. The device consists of ten $5 \times 5 \mu\text{m}^2$ sensors separated from their neighbor by $100 \mu\text{m}$.

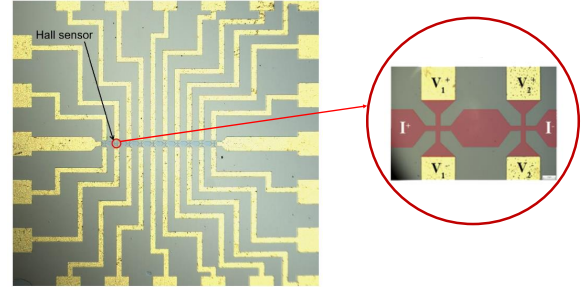


Figure Supplementary 6: A picture of the array of miniature 2DEG Hall sensors, used to detect the local magnetic field perpendicular to their plane.